DALTON

Reactions of copper pyridonate complexes with hydrated lanthanoid nitrates

Alexander J. Blake, Robert O. Gould, Craig M. Grant, Paul E. Y. Milne, Simon Parsons and Richard E. P. Winpenny*

Department of Chemistry, The University of Edinburgh, West Mains Road, Edinburgh EH9 3JJ, UK

Twenty new copper–lanthanoid complexes have been prepared. The route involves reaction of preformed copper pyridonate complexes with hydrated lanthanoid nitrates in a variety of solvents. Structural characterisation of eleven of these complexes gave some indications of how the structure is controlled in these compounds. Reaction of $[Cu_6Na(mhp)_{12}][NO_3]$ (mhp = 6-methyl-2-pyridonate) with hydrated lanthanum nitrate in CH_2Cl_2 leads to a high-nuclearity complex containing a $Cu_{12}La_8$ core. The twelve Cu atoms are arranged in a cuboctahedron surrounded by a cube of eight La atoms. Similar reactions involving 6-chloro-, 6-bromo- and 6-fluoro-2-pyridonate led to tetranuclear complexes which fall into three distinct structural groups. Consideration is given to the factors governing the choice of structural group.

A number of groups have been investigating routes to heterometallic copper–lanthanoid compounds.[1–13] Our own work[6–11] has utilised the ambidentate bridging compound 2-pyridone and 6-substituted derivatives thereof. Earlier results have indicated that the nuclearity and structure of these complexes depend on the pyridone derivative used, the solvent and the specific lanthanoid involved. For example, we have shown that reactions in MeOH lead to tetranuclear species with a Cu_2Ln_2 core if 6-methyl-2-pyridonate (mhp) is used, and to tetranuclear species with a Cu_3Ln core if 6-chloro-2-pyridonate (chp) is involved. We have also shown that reactions involving lanthanum nitrate and chp as ligand produce different metal cores if the solvent is varied from MeOH to EtOH or MeCN. From these structures and magnetic measurements we have been able to derive a magnetostructural correlation for Cu–Gd complexes,[11] demonstrating that the magnitude of the ferromagnetic exchange interaction between the different metal centres is exponentially dependent on the Cu · · · Gd distance.

Here we report investigations into several aspects of the synthesis. Characterisation of such complicated species requires X-ray crystallographic analysis, and in some cases it is possible that the crystalline product is not the major compound in the reaction. For most of the reactions reported here the crystals studied were formed in at least 20% yield, often higher. However, the limitations of using crystallography as a tool for studying reaction paths should be borne in mind. Preliminary reports involving two of the complexes have appeared.[7,8]

Experimental

Preparation of compounds

The compounds $[Cu_6Na(mhp)_{12}][NO_3]$ **1**, $[Cu_2(chp)_4]$ **2**, $[Cu_2(bhp)_4]$ **3** (bhp = 6-bromo-2-pyridonate) and $[Cu_2(fhp)_4]_2$ **4** (fhp = 6-fluoro-2-pyridonate) were prepared as described previously.[7,14] Hydrated lanthanoid nitrate salts were obtained from Aldrich or Johnson Matthey and used as obtained. All solvents were used as obtained. Analytical data and yields for compounds **6**–**25** are given in Table 1.

Mass spectra were obtained by fast-atom bombardment of samples in a 3-nitrobenzyl alcohol matrix on a Kratos MS50 spectrometer. Analytical data were obtained on a Perkin-Elmer 2400 elemental analyser by the University of Edinburgh Microanalytical Service.

Reactions of complex 1 with hydrated lanthanoid nitrates

$[Cu_{12}La_8(\mu_3\text{-}OH)_{24}(NO_3)_{21.2}(Hmhp)_{13}(H_2O)_{5.5}][NO_3]_{2.8}\cdot 2Hmhp$ 5. Compound **1** (0.05 g, 0.03 mmol) was dissolved in CH_2Cl_2 (10 cm^3) giving a deep green solution to which was added $La(NO_3)_3\cdot 6H_2O$ (0.1 g, 0.23 mmol). The solution gradually changed to pale blue over several hours and after 4 d had become colourless. During this period a small quantity of light blue crystals formed on the side of the reaction vial. These were manually separated from the residual white solid in the vial. The yield was lower than 5%. Attempts to scale-up this reaction were unsuccessful, producing pale blue powders of uncertain composition. Similar reactions involving other lanthanoid nitrates produced pale blue oils.

Reactions of complex 2 with hydrated lanthanoid nitrates in CH_2Cl_2

$[Cu_3Gd(chp)_8(NO_3)]$ 6. Compound **2** (0.684 g, 1.067 mmol) was dissolved in CH_2Cl_2 (50 cm^3) and the red solution stirred as solid $Gd(NO_3)_3\cdot 6H_2O$ (1.043 g, 2.313 mmol) was added. Over 48 h the solution changed from red to green, it was then filtered through Celite and concentrated to 15 cm^3. Diethyl ether vapour was allowed to diffuse into this solution at room temperature, producing dark green crystals of complex **6** over 2 d. These crystals were suitable for X-ray analysis. FAB mass spectrum (significant peaks, possible assignment): *m*/*z* 1377, $[Cu_3Gd(chp)_8]$; 1312 $[Cu_2Gd(chp)_8]$; 1247, $[Cu_3Gd(chp)_7]$; 1119, $[Cu_3Gd(chp)_6]$; 989, $[Cu_3Gd(chp)_5]$; 926, $[Cu_2Gd(chp)_5]$; 860, $[Cu_3Gd(chp)_4]$; 798, $[Cu_2Gd(chp)_4]$; and 705, $[Cu_3Gd(chp)_8]$.

$[Cu_3Pr(chp)_8(NO_3)]$ 7. This complex was synthesized in an identical manner to that described for **6**, with hydrated praseodymium nitrate in place of gadolinium nitrate. FAB mass spectrum: *m*/*z* 977, $[Cu_3Pr(chp)_5]$; 781, $[Cu_3Pr(chp)_3(NO_3)]$; 590, $[Cu_3Pr(chp)_2]$; and 384, $[Cu_2(chp)_2]$.

$[Cu_3Nd(chp)_8(NO_3)]$ 8. This complex was synthesized in an identical manner to that described for **6**, with hydrated neodymium nitrate in place of gadolinium nitrate. FAB mass spectrum: *m*/*z* 978, $[Cu_3Nd(chp)_5]$; 786, $[Cu_3Nd(chp)_3(NO_3)]$; 593, $[Cu_3Nd(chp)_2]$; and 384, $[Cu_2(chp)_2]$.

$[Cu_3Sm(chp)_8(NO_3)]$ 9. This complex was synthesized in an identical manner to that described for **6**, with hydrated samarium nitrate in place of gadolinium nitrate. FAB mass spectrum: *m*/*z* 986, $[Cu_3Sm(chp)_5]$; 787, $[Cu_3Sm(chp)_3(NO_3)]$; 601, $[Cu_3Sm(chp)_2]$; and 384, $[Cu_2(chp)_2]$.

$[Cu_3Er(chp)_8(NO_3)]$ 10. This complex was synthesized in an identical manner to that described for **6**, with hydrated erbium nitrate in place of gadolinium nitrate. A unit-cell determination gave a closely similar cell to that for **6**: triclinic, $a = 13.080(15)$, $b = 14.642(14)$, $c = 16.409(12)$ Å, $\alpha = 91.73(7)$, $\beta = 93.21(8)$, $\gamma = 97.79(8)°$, $U = 3106$ Å^3. No significant peaks were observed by FAB mass spectrometry.

$[Cu_3Yb(chp)_7(Hchp)(NO_3)_2]$ 11. This complex was synthesized in an identical manner to that described for **6**, with hydrated ytterbium nitrate in place of gadolinium nitrate. The crystals formed from ether diffusion into CH_2Cl_2 were suitable for X-ray analysis. FAB mass spectrum: *m*/*z* 1393, $[Cu_3Yb(chp)_7(Hchp)]$; 1263 $[Cu_3Yb(chp)_7]$; 1135, $[Cu_3Yb(chp)_6]$; 1070, $[Cu_3Yb(chp)_5(NO_3)]$; 1007, $[Cu_3Yb(chp)_5]$; 942, $[Cu_2Yb(chp)_5]$; 876, $[CuYb(chp)_5]$; and 384, $[Cu_2(chp)_2]$.

$[Cu_3Y(chp)_7(Hchp)(NO_3)_2]$ 12. This complex was synthesized in an identical manner to that described for **6**, with hydrated yttrium nitrate in place of gadolinium nitrate. A unit-cell determination gave an identical cell to that for **11**: monoclinic, $a = 19.05(3)$, $b = 13.08(3)$, $c = 24.29(4)$ Å, $\beta = 112.85(11)°$, $U = 5576$ Å^3. FAB mass spectrum: *m*/*z* 1308, $[Cu_3Y(chp)_7(Hchp)]$; 1178 $[Cu_3Y(chp)_7]$; 1050, $[Cu_3Y(chp)_6]$; 920, $[Cu_3Y(chp)_5]$; 859, $[Cu_2Y(chp)_5]$; 791, $[Cu_3Y(chp)_4]$; 729, $[Cu_2Y(chp)_4]$; 601, $[Cu_2Y(chp)_3]$; and 538, $[CuY(chp)_3]$.

Reactions of complex 2 with hydrated lanthanoid nitrates in tetrahydrofuran (thf)

$[\{CuYb(\mu\text{-}OH)(chp)_2(NO_3)_2(H_2O)_2\}_2]$ 13. Compound **2** (0.073 g, 0.114 mmol) was dissolved in thf (10 cm^3) and solid $Yb(NO_3)_3{\cdot}5H_2O$ (0.118 g, 0.263 mmol) added. The solution changed immediately from red to light green. After 24 h it was filtered and crystallisation achieved by diffusion of diethyl ether into the solution at room temperature. Large green needles suitable for X-ray diffraction analysis formed over 24 h. No significant peaks were observed by FAB mass spectrometry.

$[\{CuEr(\mu\text{-}OH)(chp)_2(NO_3)_2(H_2O)_2\}_2]$ 14. This complex was synthesized in an identical manner to that described for **13**, with hydrated erbium nitrate in place of ytterbium nitrate. Crystallisation was accomplished by slow addition of hexane to the solution. A unit-cell determination gave an identical cell to that for **13**: monoclinic, $a = 12.79(2)$, $b = 15.69(2)$, $c = 17.26(2)$ Å, $\beta = 103.3(2)°$, $U = 3371$ Å^3. No significant peaks were observed by FAB mass spectrometry.

Reactions of complex 2 with hydrated lanthanoid nitrates in CH_2Cl_2–MeOH

$[\{CuYb(\mu\text{-}OMe)(chp)_2(NO_3)_2(MeOH)_2\}_2]$ 15. Compound **2** (1 g, 1.7 mmol) was dissolved in CH_2Cl_2 (100 cm^3) and a solution of $Yb(NO_3)_3{\cdot}5H_2O$ (1.5 g, 3.4 mmol) in MeOH (20 cm^3) added dropwise. The solution became green and was filtered then evaporated to dryness, leaving a green tar. This was redissolved in methanol (15 cm^3), filtered and diethyl ether vapour allowed to diffuse into the solution over a period of 1 week giving light green crystals suitable for X-ray analysis.

Reactions of complex 3 with hydrated lanthanoid nitrates in CH_2Cl_2

$[Cu_3Sm(bhp)_8(NO_3)]$ 16. This complex was synthesized in an identical manner to that described for **6**, using **3** in place of **2** and hydrated samarium nitrate in place of gadolinium nitrate. FAB mass spectrum: *m*/*z* 1550, $[Cu_3Sm(bhp)_7]$; 1380, $[Cu_3Sm(bhp)_6]$; 1206, $[Cu_3Sm(bhp)_5]$; 1142, $[Cu_2Sm(bhp)_5]$; 968, $[Cu_2Sm(bhp)_4]$.

$[Cu_3Gd(bhp)_8(NO_3)]$ 17. This complex was synthesized in an identical manner to that described for **6**, using **3** in place of **2**. FAB mass spectrum: *m*/*z* 1557, $[Cu_3Gd(bhp)_7]$; 1386, $[Cu_3Gd(bhp)_6]$; 1212, $[Cu_3Gd(bhp)_5]$; 1149, $[Cu_2Gd(bhp)_5]$; and 976, $[Cu_2Gd(bhp)_4]$.

$[\{CuEr(\mu\text{-}OH)(bhp)_2(NO_3)_2(Hbhp)_2\}_2]$ 18. This complex was synthesized in an identical manner to that described for **6**, using **3** in place of **2** and hydrated erbium nitrate in place of gadolinium nitrate. Single crystals suitable for X-ray diffraction studies were grown by diffusion of ether vapour into a solution in CH_2Cl_2. No significant peaks were observed by FAB mass spectrometry.

Reactions of complex 3 with hydrated lanthanoid nitrates in CH_2Cl_2–MeOH

$[\{CuPr(\mu\text{-}OMe)(bhp)_2(NO_3)_2(MeOH)_3\}_2]$ 19. Compound **3** (0.186 g, 0.227 mmol) was dissolved in CH_2Cl_2 (30 cm^3) and a solution of $Pr(NO_3)_3{\cdot}6H_2O$ (0.227 g, 0.552 mmol) in MeOH (6 cm^3) added dropwise, resulting in a change from red to light green. The solution was stirred for 24 h then concentrated *in vacuo* to leave a tar-like residue. This was redissolved in MeOH (20 cm^3) to give a green solution which was filtered through Celite. Crystallisation could be achieved either by diffusion of diethyl ether vapour into this solution, or by allowing the solution to evaporate slowly at room temperature. No significant peaks were observed by FAB mass spectrometry.

$[\{CuNd(\mu\text{-}OMe)(bhp)_2(NO_3)_2(MeOH)_3\}_2]$ 20. This complex was synthesized in an identical manner to that described for complex **18**, with hydrated neodymium nitrate in place of praseodymium nitrate. Crystallisation was accomplished by allowing the solution to evaporate slowly at room temperature. A unit-cell determination gave an identical cell to that for **19**: triclinic, $a = 8.731(10)$, $b = 12.14(2)$, $c = 14.10(2)$ Å, $\alpha = 114.31(10)$, $\beta = 99.06(9)$, $\gamma = 92.75(10)°$, $U = 1334$ Å^3. No significant peaks were observed by FAB mass spectrometry.

$[\{CuGd(\mu\text{-}OMe)(bhp)_2(NO_3)_2(MeOH)_2\}_2]$ 21. This complex was synthesized in an identical manner to that described for **18**, with hydrated gadolinium nitrate in place of praseodymium nitrate. Crystals suitable for X-ray analysis were grown by allowing the solvent to evaporate slowly at room temperature. FAB mass spectrum: *m*/*z* 976, $[Cu_2Gd(bhp)_4]$; and 629, $[Cu_2Gd(bhp)_2]$.

$[\{CuEr(\mu\text{-}OMe)(bhp)_2(NO_3)_2(MeOH)_2\}_2]$ 22. This complex was synthesized in an identical manner to that described for **18**, with hydrated erbium nitrate in place of praseodymium nitrate. Crystals suitable for X-ray analysis were grown by allowing the solvent to evaporate slowly at room temperature. FAB mass spectrum: *m*/*z* 1214, $[Cu_2Er_2(OMe)(bhp)_4]$; and 986, $[Cu_2Er(bhp)_4]$.

Reactions of complex 4 with hydrated lanthanoid nitrates in CH_2Cl_2–MeOH

$[\{CuPr(fhp)_4(NO_3)(MeOH)\}_2]$ 23. Compound **4** (0.348 g, 0.303 mmol) was dissolved in CH_2Cl_2 (60 cm^3) and a solution of $Pr(NO_3)_3{\cdot}6H_2O$ (0.272 g, 0.625 mmol) in MeOH (20 cm^3) added dropwise. The dark green solution lightened during this procedure. It was then stirred for 24 h before being concentrated *in vacuo* to leave a tar-like residue. This was redissolved in MeOH (30 cm^3) to give a green solution which was filtered through Celite. Crystallisation was achieved by allowing the solvent to evaporate slowly at room temperature. Crystals were obtained in 2 d. FAB mass spectrum: *m*/*z* 1194, $[Cu_2Pr_2(fhp)_7]$; 716, $[Cu_2Pr(fhp)_4]$; and 541, $[CuPr(fhp)_3]$.

Table 1 Analytical data for compounds **6**–**25**

Complex		Analysis (%)*			
		C	H	N	Yield (%)
6	$[Cu_3Gd(chp)_8(NO_3)]$	33.9 (33.4)	2.0 (1.7)	7.9 (8.8)	56
7	$[Cu_3Pr(chp)_8(NO_3)]$	33.7 (33.8)	2.3 (1.7)	8.6 (8.9)	32
8	$[Cu_3Nd(chp)_8(NO_3)]$	31.9 (32.3)	1.9 (1.7)	8.7 (9.4)	24
9	$[Cu_3Sm(chp)_8(NO_3)]$	33.5 (33.5)	1.9 (1.7)	8.6 (8.8)	33
10	$[Cu_3Er(chp)_8(NO_3)]$	33.5 (33.2)	2.0 (1.7)	9.1 (8.7)	39
11	$[Cu_3Yb(chp)_7(Hchp)(NO_3)_2]$	31.6 (31.7)	1.2 (1.6)	8.7 (9.2)	33
12	$[Cu_3Y(chp)_7(Hchp)(NO_3)_2]$	33.3 (33.5)	1.9 (1.7)	9.3 (9.8)	22
13	$[\{CuYb(\mu\text{-}OH)(chp)_2(NO_3)_2(H_2O)_2\}_2]\cdot 2thf$	24.3 (22.6)	2.8 (2.6)	6.6 (7.5)	26
14	$[\{CuEr(\mu\text{-}OH)(chp)_2(NO_3)_2(H_2O)_2\}_2]$	22.0 (22.8)	2.5 (2.6)	7.4 (7.6)	15
15	$[\{CuYb(\mu\text{-}OMe)(chp)_2(NO_3)_2(MeOH)_2\}_2]$	20.8 (22.0)	7.6 (7.9)	2.4 (2.4)	20
16	$[Cu_3Sm(bhp)_8(NO_3)]$	26.2 (26.9)	1.6 (1.3)	7.4 (7.1)	21
17	$[Cu_3Gd(bhp)_8(NO_3)]$	25.8 (26.8)	1.3 (1.3)	7.4 (7.0)	25
18	$[\{CuEr(\mu\text{-}OH)(bhp)_2(NO_3)_2(Hbhp)_2\}_2]$	21.0 (22.9)	1.5 (1.4)	7.7 (8.0)	21
19	$[CuPr(\mu\text{-}OMe)(bhp)_2(NO_3)_2(MeOH)_3\}_2]$	21.6 (21.0)	3.0 (2.6)	6.9 (7.0)	11
20	$[\{CuNd(\mu\text{-}OMe)(bhp)_2(NO_3)_2(MeOH)_3\}_2]$	18.6 (20.9)	2.2 (2.5)	7.1 (7.0)	16
21	$[\{CuGd(\mu\text{-}OMe)(bhp)_2(NO_3)_2(MeOH)_2\}_2]$	20.2 (21.4)	1.9 (2.2)	6.8 (7.1)	30
22	$[\{CuEr(\mu\text{-}OMe)(bhp)_2(NO_3)_2(MeOH)_2\}_2]$	17.8 (19.6)	2.1 (1.9)	7.1 (7.0)	16
23	$[\{CuPr(fhp)_4(NO_3)(MeOH)\}_2]$	33.3 (33.8)	1.9 (2.1)	8.4 (9.4)	12
24	$[\{CuGd(fhp)_4(NO_3)(MeOH)\}_2]$	32.4 (33.0)	1.8 (2.1)	9.3 (9.2)	14
25	$[\{CuYb(fhp)_4(NO_3)(MeOH)\}_2]$	29.3 (32.4)	1.8 (2.1)	9.3 (9.0)	22

* Calculated values are given in parentheses.

$[\{CuGd(fhp)_4(NO_3)(MeOH)\}_2]$ 24. This complex was synthesized in an identical manner to that described for **23**, with hydrated gadolinium nitrate in place of ytterbium nitrate. A unit-cell determination gave an identical cell to that for **23**: monoclinic, $a = 24.23(2)$, $b = 12.38(2)$, $c = 19.76(2)$ Å, $\beta = 111.6(2)°$, $U = 5535$ Å^3. No significant peaks were observed by FAB mass spectrometry.

$[\{CuYb(fhp)_4(NO_3)(MeOH)\}_2]$ 25. This was synthesized in an identical manner to that described for **23**, with hydrated ytterbium nitrate in place of praseodymium nitrate. Crystals suitable for X-ray analysis were grown by allowing the solvent to evaporate slowly at room temperature. No significant peaks were observed by FAB mass spectrometry.

Crystallography

Crystal data and data collection and refinement parameters for compounds **5**, **6**, **11**, **13**, **15**, **18**, **19**, **21**–**23** and **25** are given in Table 2, selected bond lengths and angles in Tables 3–8.

Data collection and processing. Data for all complexes except **23** were collected on a Stoë Stadi-4 four-circle diffractometer. Those for **23** were collected on a Siemens SMART-CCD three-circle diffractometer. Data for **5** and **13** were collected with graphite-monochromated Mo-Kα radiation (λ = 0.710 73 Å) at room temperature, all other data at 150.0(2) K, with the crystals cooled using an Oxford Cryosystems low-temperature device.[17] Data for **11**, **13**, **18**, **19**, **21** and **25** were collected using ω–θ scans, **5** and **15** using ω–2θ scans, and for **6** and **22** using ω scans. On-line profile fitting[18] was used during data collection for **11**, **15**, **19** and **21**. All data were corrected for Lorentz-polarisation factors. Semiempirical absorption corrections based on azimuthal measurements were applied to data for all compounds; DIFABS[19] was applied to data for compounds **6**, **13**, **18** and **22** to allow for large absorption effects due to lanthanoid atoms and Br atoms in **18** and **22**. No significant decay occurred during data collection for any compound.

Structure analysis and refinement. All structures were solved by heavy-atom methods using SHELXS 86[20] which revealed the position of the copper and lanthanoid atoms in all cases and additionally the Br atoms in complexes **18**, **19**, **21** and **22**. The structures were completed by iterative cycles of ΔF syntheses and full-matrix least-squares refinement; **5** and **15** were refined against F using SHELX 76,[15] all others against F^2 with SHELXL 93.[16] All full-weight non-hydrogen atoms were refined anisotropically in all structures except **11** and **25** where only the metal atoms were so refined. Hydrogen atoms were included in idealised positions [C–H 0.96 Å for ring, 0.98 Å for methyl, O–H 0.90 Å], and assigned isotropic thermal parameters [U(H) = 1.2 U_{eq}(C) for aromatic, U 1.5 U_{eq}(C) for methyl, U 1.5 U_{eq}(O) for hydroxyl or water]. Complex **11** displayed considerable disorder in the coordinated nitrate groups. Each nitrate has one full-occupancy oxygen atom with the remaining atoms disordered with 50% occupancies over two sites. Corresponding N–O distances were restrained to be equal and each nitrate fragment was restrained to be flat. All half-occupancy atoms were refined isotropically.

Atomic coordinates, thermal parameters, and bond lengths and angles have been deposited at the Cambridge Crystallographic Data Centre (CCDC). See Instructions for Authors, *J. Chem. Soc.*, *Dalton Trans.*, 1997, Issue 1. Any request to the CCDC for this material should quote the full literature citation and the reference number 186/331.

Results

Previous reports of reactions of copper pyridonate complexes with lanthanoid complexes have shown that several different structural types can be formed.[7–11] For three structural types[7,9] only one example of each has been found, while another two types have occurred frequently.[10,11] These two common structures have both been synthesized in CH_2Cl_2–MeOH, and contain either a Cu_2Ln_2 core,[10] where the copper centres are bridged by two OMe groups, or a Cu_3Ln core,[11] where the solvent has much less involvement. Whether the former, 'Type I', complexes or the latter, 'Type II', complexes are formed appears to be somewhat dependent on the pyridone ligand used; Type I complexes have generally involved mhp,[10] Type II complexes chp bridges.[11] Here we have carried out reactions using Hmhp, Hchp, Hbhp and Hfhp in a range of solvents in an attempt to rationalise this reactivity.

Synthesis and structure of $[Cu_{12}La_8(\mu_3\text{-}OH)_{24}(NO_3)_{21.2}(Hmhp)_{13}(H_2O)_{5.5}][NO_3]_{2.8}\cdot 2Hmhp$ 5

The highest-nuclearity mixed Cu–Ln complex **5** results from reaction of **1** with solid hydrated lanthanum nitrate in CH_2Cl_2.

Table 2 Experimental data for the X-ray diffraction studies of compounds **5**, **6**, **11**, **13**, **15**, **18**, **19**, **21**–**23** and **25**

	5	**6**	**11**	**13**	**15**	**18**
Formula	$C_{91}H_{142}Cl_2Cu_{12}$-$La_8N_{39}O_{116.5}$	$C_{40}H_{24}Cl_8GdN_9$-$O_{11}\cdot C_4H_{10}O\cdot$ $H_2O\cdot 0.5CH_2Cl_2$	$C_{40}H_{25}Cl_8Cu_3$-$N_{10}O_{14}Yb_2\cdot$ $0.78CH_2Cl_2$	$C_{20}H_{22}Cl_4Cu_2N_8$-$O_{22}Yb_2\cdot 2C_4H_8O$	$C_{26}H_{30}Cl_4Cu_2N_8$-$O_{22}Yb_2\cdot CH_4O\cdot$ $2C_4H_{10}O$	$C_{40}H_{30}Br_8Cu_2$-$Er_2N_{12}O_{22}$
M	5590.4	1569.7	1581.9	1483.6	1605.2	2131.6
Crystal system	Monoclinic	Triclinic	Monoclinic	Monoclinic	Triclinic	Triclinic
Space group	$P2_1/n$	$P\bar{1}$	$P2_1/n$	$P2_1/n$	$P\bar{1}$	$P\bar{1}$
a/Å	15.4628(21)	13.247(13)	18.990(10)	12.868(13)	8.601(8)	10.856(13)
b/Å	32.535(5)	14.555(13)	13.063(7)	16.40(2)	13.436(10)	11.70(2)
c/Å	18.469(3)	16.35(2)	24.256(13)	16.72(2)	25.584(10)	13.39(2)
α/°		91.36(8)			92.840(6)	106.14(10)
β/°	98.725(18)	93.45(7)	112.84(5)	103.90(8)	91.000(8)	95.78(10)
γ/°		98.31(12)			104.100(6)	113.93(9)
U/Å	9186	3112	5545	3426	2862	1448
No. reflections	40	41	18	10	23	9
2θ/°	21–22	25–35	25–30	16–25	27–28	25–27
Z	2[a]	2	4	2[a]	2	1[a]
D_c/g cm^{-3}	2.02	1.68	1.90	1.44	1.86	2.445
F(000)	5380	1544	3085	1436	1460	1004
Crystal size/mm	0.14 × 0.14 × 0.21	0.43 × 0.35 × 0.19	0.30 × 0.25 × 0.15	0.75 × 0.20 × 0.10	0.31 × 0.31 × 0.89	0.23 × 0.08 × 0.08
Crystal shape and colour	Blue triangular prism	Green prism	Dark green rhomb	Emerald-green lath	Green column	Emerald-green block
Mounting	Glass fibre	Oil drop	Oil drop	Mother-liquor in capillary	Oil drop on glass fibre	Oil drop on glass fibre
μ/mm^{-1}	3.33	2.51	3.34	3.54	4.23	9.20
2θ maximum for data collection/°	45	42	45	50	45	45
Unique data	12 233	6682	7224	5980	7323	3799
Observed data [$I > 2\sigma(I)$]	6435	5507	5354	2176	6489	2287
Maximum Δ/σ ratio	0.001	0.003	0.013	0.001	0.047	0.003
*R*1, *wR*2[b]		0.0661, 0.2043	0.0416, 0.1292	0.0753, 0.2843		0.0559, 0.1571
R, *R*′[c]	0.0838, 0.0986				0.0546, 0.0636	
Weighting scheme, w^{-1}[d]	$\sigma^2(F)$ + 0.000 91F^2	$\sigma^2(F_o^2)$ +(0.122P)^2 + 46.61P	$\sigma^2(F_o^2)$ + (0.0399P)^2 + 53.16P	$\sigma^2(F_o^2)$ + (0.1259P)^2	$\sigma^2(F)$ + 0.000 076F^2	$\sigma^2(F_o^2)$+ (0.0869P)^2
Goodness of fit	1.048	1.038	1.014	0.923	0.795	1.024
Largest residuals/ e Å^{-3}	+1.34, −1.12	+2.128, −1.338	+1.325, −0.638	+1.075, −1.038	+1.47, −1.34	+1.726, −1.611

(*continued*)

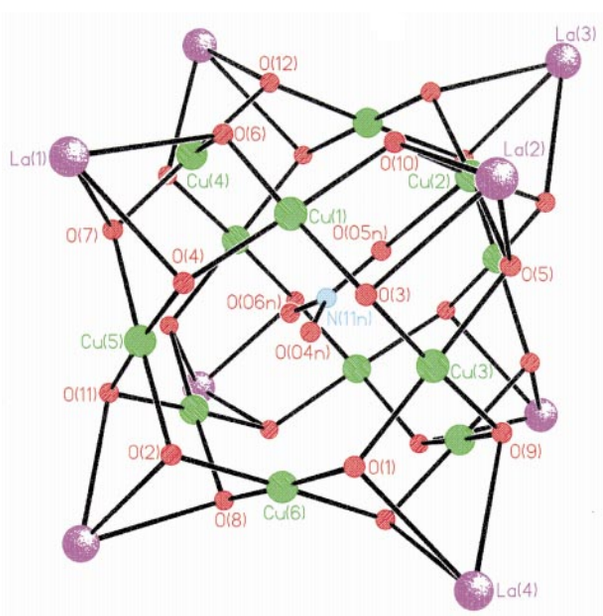

Fig. 1 The $[Cu_{12}La_8(\mu_3\text{-}OH)_{24}(NO_3)]^{23+}$ core of complex **5**: La, purple; Cu, green; N, blue; O, red

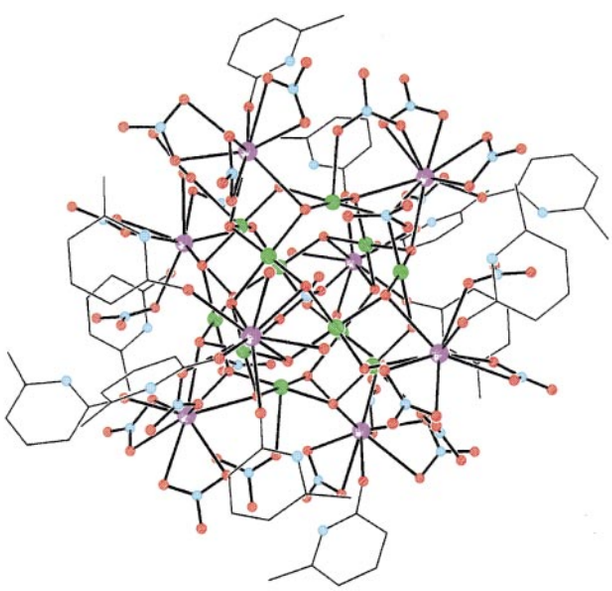

Fig. 2 Structure of complex **5** in the crystal. Colours as for Fig. 1

Small quantities of blue crystals grow while the initially dark green solution decolorises over 4 d. Structural analysis reveals a central hydroxide-bridged core incorporating a cuboctahedron of copper centres inside a cube of eight lanthanums, which implies the core has non-crystallographic O_h symmetry (Fig. 1). This ordered inorganic core is surrounded by a sheath of disordered organic material (Fig. 2).

The $Cu_{12}La_8$ core is held together by twenty-four μ_3-hydroxides. The structure can be envisaged as consisting of eight $LaCu_3$ tetrahedra, with each Cu part of two such tetra-

Table 2 (*continued*)

	19	**21**	**22**	**23**	**25**
Formula	$C_{28}H_{34}Br_4Cu_2N_8O_{24}Pr_2\cdot 2CH_4O$	$C_{26}H_{26}Br_4Cu_2Gd_2N_8O_{22}$	$C_{26}H_{26}Br_4Cu_2Er_2N_8O_{22}\cdot 2C_4H_{10}O\cdot CH_4O$	$C_{42}H_{32}Cu_2F_8N_{10}O_{16}Pr_2\cdot 1.6CH_4O$	$C_{42}H_{32}Cu_2F_8N_{10}O_{16}Yb_2\cdot H_2O$
M	1659.3	1571.8	1772.1	1536.5	1573.9
Crystal system	Triclinic	Monoclinic	Triclinic	Monoclinic	Monoclinic
Space group	$P\bar{1}$	$P2_1/n$	$P\bar{1}$	$C2/c$	$C2/c$
a/Å	8.749(4)	12.977(3)	8.612(14)	24.3163(14)	24.65(2)
b/Å	12.136(4)	14.057(3)	13.516(20)	12.5621(8)	12.301(9)
c/Å	14.129(4)	13.282(2)	25.69(4)	19.766(12)	19.444(13)
α/°	114.11(6)		92.2(2)		—
β/°	98.99(3)	111.306(19)	91.74(11)	111.586(10)	110.89(6)
γ/°	92.85(3)		104.14(19)		—
U/Å^3	1342	1496	2895	5614	5507
No. reflections	40	40	14	—	34
2θ/°	24–31	17–28	29–30	—	20–27
Z	1[a]	2[a]	1[a]	4[a]	4[a]
D_c/g cm^{-3}	2.054	2.313	2.033	1.82	1.898
F(000)	802	1496	1716	3002	3040
Crystal size/mm	0.25 × 0.19 × 0.19	0.27 × 0.27 × 0.23	0.58 × 0.12 × 0.12	0.21 × 0.26 × 0.4	0.27 × 0.39 × 0.12
Crystal shape and colour	Green cube	Small green block	Green column	Dark green block	Dark green block
Mounting	Oil drop on glass fibre	Oil drop on glass fibre	Oil drop on glass fibre	Oil drop on glass fibre	Oil drop on glass fibre
μ/mm^{-1}	5.63	7.456	6.436	2.55	4.23
2θ maximum for data collection/°	50	45	45	45	42
Unique data	4734	2922	7588	4003	3611
Observed data [$I > 2\sigma(I)$]	3814	2386	5333	3755	2262
Maximum Δ/σ ratio	0.001	0.000	0.006	0.009	0.001
$R1$, $wR2$[b] R, R'[c]	0.0390, 0.0962	0.0382, 0.0981	0.0591, 0.1730	0.049, 0.1110	0.1132, 0.2505
Weighting scheme, w^{-1}[d]	$\sigma^2(F_o^2) + (0.0410P)^2 + 0.056P$	$\sigma^2(F_o^2) + (0.0587P)^2 + 2.1254P$	$\sigma^2(F_o^2) + (0.0814P)^2 + 49.65P$	$\sigma^2(F_o^2) + (0.0451P)^2 + 51.89P$	$\sigma^2(F_o^2) + (0.0484P)^2 + 748.8P$
Goodness of fit	1.056	1.048	0.031	1.147	1.104
Largest residuals/ e Å^{-3}	+0.78, −0.08	+1.040, −0.060	+2.463, −2.454	+0.844, −1.923	+1.958, −2.143

[a] The molecule lies on an inversion centre. [b] Refinement against F^2, SHELXL 93.[16] $R1 = \Sigma |F_o - F_c|/\Sigma F_o$ and $wR2 = [\Sigma w(F_o^2 - F_c^2)^2/\Sigma w(F_o)^2]^{\frac{1}{2}}$. [c] Refinement against F, SHELX 76.[15] [d] $P = \frac{1}{3}(2F_c^2 + F_o^2)$.

Table 3 Bond lengths (Å) and angles (°) about copper sites in compound **5**

Cu(1)–O(3)	1.976(14)	Cu(4)–O(6)	1.933(14)	Cu(2)–O(42n)	2.466(17)	Cu(5)–O(11)	1.974(14)
Cu(1)–O(4)	1.952(13)	Cu(4)–O(7)	1.923(14)	Cu(2)–O(05n)	2.40(4)	Cu(5)–O(05n′)	2.52(4)
Cu(1)–O(6)	1.955(14)	Cu(4)–O(9′)	1.953(14)	Cu(2)–O(06n′)	2.46(3)	Cu(6)–O(1)	1.980(14)
Cu(1)–O(10)	1.939(13)	Cu(4)–O(12)	1.932(15)	Cu(3)–O(1)	1.965(14)	Cu(6)–O(2)	1.982(13)
Cu(2)–O(5)	1.983(14)	Cu(4)–O(52n)	2.376(18)	Cu(3)–O(3)	1.943(14)	Cu(6)–O(8)	1.935(14)
Cu(2)–O(8′)	1.917(14)	Cu(5)–O(2)	1.949(13)	Cu(3)–O(5)	1.967(14)	Cu(6)–O(12′)	1.983(15)
Cu(2)–O(10)	1.976(13)	Cu(5)–O(4)	1.994(13)	Cu(3)–O(9)	1.965(14)	Cu(6)–O(33n)	2.409(20)
Cu(2)–O(11′)	1.961(14)	Cu(5)–O(7)	1.984(14)	Cu(3)–O(06n′)	2.52(3)		
O(3)–Cu(1)–O(4)	96.0(6)	O(3)–Cu(1)–O(6)	177.4(6)	O(5)–Cu(3)–O(9)	92.7(6)	O(5)–Cu(3)–O(06n′)	78.2(9)
O(3)–Cu(1)–O(10)	84.7(5)	O(4)–Cu(1)–O(6)	85.8(6)	O(9)–Cu(3)–O(06n′)	95.2(9)	O(6)–Cu(4)–O(7)	85.8(6)
O(4)–Cu(1)–O(10)	177.8(6)	O(6)–Cu(1)–O(10)	93.4(6)	O(6)–Cu(4)–O(9′)	177.8(6)	O(6)–Cu(4)–O(12)	93.8(6)
O(5)–Cu(2)–O(8′)	175.9(6)	O(5)–Cu(2)–O(10)	83.0(5)	O(6)–Cu(4)–O(52n)	105.3(6)	O(7)–Cu(4)–O(9′)	94.7(6)
O(5)–Cu(2)–O(11′)	97.3(6)	O(5)–Cu(2)–O(42n)	103.3(6)	O(7)–Cu(4)–O(12)	179.2(6)	O(7)–Cu(4)–O(52n)	91.5(6)
O(5)–Cu(2)–O(05n)	101.9(9)	O(5)–Cu(2)–O(06n′)	79.5(9)	O(9′)–Cu(4)–O(12)	85.7(6)	O(9′)–Cu(4)–O(52n)	76.9(6)
O(8′)–Cu(2)–O(10)	99.9(6)	O(8′)–Cu(2)–O(11′)	80.0(6)	O(12)–Cu(4)–O(52n)	89.3(6)	O(2)–Cu(5)–O(4)	94.0(5)
O(8′)–Cu(2)–O(42n)	79.4(6)	O(8′)–Cu(2)–O(05n)	74.8(9)	O(2)–Cu(5)–O(7)	178.1(6)	O(2)–Cu(5)–O(11)	85.7(6)
O(8′)–Cu(2)–O(06n′)	97.9(9)	O(10)–Cu(2)–O(11′)	176.7(6)	O(2)–Cu(5)–O(05n′)	84.8(9)	O(4)–Cu(5)–O(7)	86.8(6)
O(10)–Cu(2)–O(42n)	95.0(5)	O(10)–Cu(2)–O(05n)	101.8(9)	O(4)–Cu(5)–O(11)	176.0(6)	O(4)–Cu(5)–(05n′)	97.9(9)
O(10)–Cu(2)–O(06n′)	82.6(9)	O(11′)–Cu(2)–O(42n)	81.7(6)	O(7)–Cu(5)–O(11)	93.4(6)	O(7)–Cu(5)–O(05n′)	93.3(9)
O(11′)–Cu(2)–O(05n)	81.4(9)	O(11′)–Cu(2)–O(06n′)	100.7(9)	O(11)–Cu(5)–O(05n′)	78.1(9)	O(1)–Cu(6)–O(2)	97.6(6)
O(42n)–Cu(2)–O(05n)	151.2(9)	O(42n)–Cu(2)–O(06n′)	176.1(9)	O(1)–Cu(6)–O(8)	175.6(6)	O(1)–Cu(6)–O(12′)	85.3(6)
O(05n)–Cu(2)–O(06n′)	28.0(11)	O(1)–Cu(3)–O(3)	94.5(6)	O(1)–Cu(6)–O(33n)	95.1(6)	O(2)–Cu(6)–O(8)	85.3(6)
O(1)–Cu(3)–O(5)	179.8(6)	O(1)–Cu(3)–O(9)	87.3(6)	O(2)–Cu(6)–O(12′)	177.1(6)	O(2)–Cu(6)–O(33n)	99.2(6)
O(1)–Cu(3)–O(06n ′)	101.5(9)	O(3)–Cu(3)–O(5)	85.6(6)	O(8)–Cu(6)–O(12′)	91.9(6)	O(8)–Cu(6)–O(33n)	87.7(6)
O(3)–Cu(3)–O(9)	176.2(6)	O(3)–Cu(3)–O(06n′)	87.8(9)	O(12′)–Cu(6)–O(33n)	80.2(6)		

hedra, and with an OH group at the centre of each $LaCu_2$ triangular face (Fig. 1). Each copper is bound to a square plane of four OH groups (Table 3). Further, longer contacts are found to a disordered nitrate anion encapsulated inside the polymetallic core, or to nitrate anions co-ordinated to La atoms. Thus, while Cu(1) is four-co-ordinate, Cu(3), Cu(4), Cu(5) and Cu(6) each have one further long contact to an O-donor (2.38–2.52 Å), while Cu(2) has two further contacts of *ca.* 2.43 Å.

Table 4 Bond lengths (Å) about lanthanum sites in compound **5**

La(1)–O(4)	2.590(13)	La(3)–O(8′)	2.508(14)
La(1)–O(6)	2.631(14)	La(3)–O(11′)	2.594(13)
La(1)–O(7)	2.607(14)	La(3)–O(1r)	2.386(16)
La(1)–O(4r)	2.399(16)	La(3)–O(11n)	2.646(18)
La(1)–O(51n)	2.622(19)	La(3)–O(13n)	2.610(18)
La(1)–O(61n)	2.658(19)	La(3)–O(21n)	2.639(16)
La(1)–O(63n)	2.766(17)	La(3)–O(23n)	2.671(17)
La(1)–O(71n)	2.609(17)	La(3)–O(31n)	2.595(18)
La(1)–O(72n)	2.593(17)	La(3)–O(42n)	2.718(17)
La(1)–O(81n)	2.557(17)	La(4)–O(1)	2.716(14)
La(2)–O(3)	2.671(14)	La(4)–O(9)	2.608(14)
La(2)–O(5)	2.588(14)	La(4)–O(12′)	2.599(14)
La(2)–O(10)	2.575(13)	La(4)–O(13a)	2.45(3)
La(2)–O(13)	2.592(20)	La(4)–O(15a)	2.68(4)
La(2)–O(14)	2.601(20)	La(4)–O(5r)	2.365(20)
La(2)–O(7r)	2.470(20)	La(4)–O(91n)	2.58(3)
La(2)–O(2r)	2.357(21)	La(4)–O(93n)	2.54(3)
La(2)–O(3r)	2.436(21)	La(4)–O(01n)	2.817(21)
La(2)–O(41n)	2.637(20)	La(4)–O(03n)	2.86(3)
La(3)–O(2′)	2.678(13)	La(4)–O(15)	2.67(6)

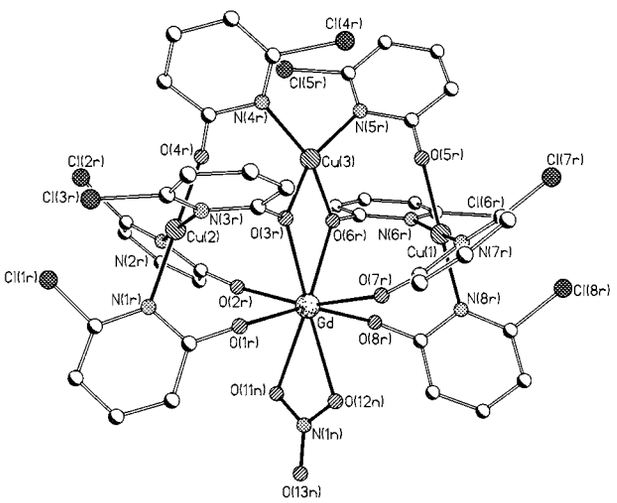

Fig. 3 Structure of complex **6** in the crystal, with the numbering scheme adopted

These additional contacts are in approximately apical positions of a square pyramid or tetragonally elongated octahedron.

The lanthanum sites are each bound to three μ_3-OH groups, with the remaining co-ordination sites occupied by a variety of ligands. Atom La(1) is ten-co-ordinate, with the additional seven sites occupied by one terminal Hmhp ligand and two bi- and two mono-dentate nitrates. Atom La(2) is nine-co-ordinate, with the six additional sites occupied by three terminal Hmhp ligands, two water molecules and a monodentate nitrate. Atom La(3) is ten-co-ordinate, with a co-ordination sphere similar to that of La(1), while the environment of La(4) is disordered, occupied by one ordered pyridonate, three bidentate nitrates and one quarter-occupancy water molecule. Even with this disorder the La–O bond lengths show a dependence on the nature of the O-donor (Table 4). The bonds to Hmhp moieties are shortest, between 2.37 and 2.47 Å, with bonds to hydroxide or water longest, between 2.57 and 2.72 Å. The La-O (nitrate) bonds show a much wider range (2.45–2.86 Å). The geometries of these lanthanum sites are irregular.

The La_8 and Cu_{12} cages show little distortion from the ideal polyhedra. The La · · · La distances within the cube vary from 6.301 to 6.705(2) Å, with the La · · · La · · · La angles at the corners of the cube varying from 86.7 to 93.3(4)°. The Cu · · · Cu contacts within the cuboctahedron are also largely invariant, ranging from 3.204 to 3.460(3) Å, and the polyhedral angles at each Cu are between 57.3 and 62.6(5)°, compared with the 60° required for a perfect cuboctahedron. The Cu · · · Ln contacts between the two polyhedra vary from 3.458 to 3.625(3) Å. The twenty-four bridging hydroxides are all pyramidal, with the sum of the bond angles varying from 311.7 to 322.2(8)°. In each case the Cu–O–Cu angle at the μ_3-OH is more obtuse than the two Cu–O–Ln angles. The range for the former varies from 109.7 to 125.5(8)°, while for the latter it is 96.0 to 105.5(8)°.

The structure of complex **5** is intriguing, but we have been unable to synthesize analogous compounds with any other 4f elements, nor to increase the yield of **5** beyond a few crystals in any one reaction. Although reasonable yields of blue powders can be obtained by adding further quantities of **1** to the reaction solution and repeating the decolorisation step, characterisation of this blue powder indicates it contains a different polymetallic compound. This might imply that **5** is an attractive curiosity, however recent results from Chen *et al.*[13] using derivatives of betaine ($NMe_3CH_2CO_2$) have involved a series of octadecanuclear complexes containing $Cu_{12}Ln_6$ cores (Ln = Sm or Gd). The copper atoms are again arranged in a cuboctahedron while the six lanthanoid sites are now describing an octahedron. The occurrence of a Cu_{12} cuboctahedron bridged by hydroxides in both **5** and the compounds reported by Chen *et al.* is surprising in that such a polyhedron has never been reported for homometallic complexes of copper(II). The Cu · · · Cu contacts in the $Cu_{12}Ln_6$ compounds fall within the same range as those in **5**. The lanthanum polyhedron in **5** involves placing lanthanum 'caps' on the triangular faces of the copper cuboctahedron; in $Cu_{12}Ln_6$ the lanthanoid atoms cap the square faces of the cuboctahedron. There is no obvious explanation for this difference.

Reactions of complex 2 with lanthanoid nitrates

The formation of complex **5** is dependent on the absence of MeOH. In the presence of MeOH, Type I Ln_2Cu_2 complexes result when **1** is treated with $Ln(NO_3)_3.xH_2O$.[10] We were therefore interested to see whether exclusion of MeOH from reactions involving **2** with lanthanoid nitrates might also lead to new structural types. Previous work with lanthanum nitrate showed that Cu–La structures showed a strong dependence on solvent.[9]

Addition of solid lanthanoid nitrates to solutions of complex **2** in CH_2Cl_2 led to Type II complexes with Cu_3Ln cores for all 4f elements from praseodymium to ytterbium and also for the 4d-metal yttrium. The structures of two of these complexes, **6** and **11**, have been determined; the remaining complexes are assumed to be isostructural with either **6** or **11** based on elemental analysis in all cases, mass spectroscopic results in all cases bar **10** (see below) and unit-cell determinations for **10** and **12**.

The structure of $[Cu_3Gd(chp)_8(NO_3)]$ **6** is shown in Fig. 3 and selected bond lengths and angles are given in Table 5. A Cu_3Gd core is bridged by eight chp ligands with a terminal bidentate nitrate group attached to the Gd atom. There is a non-crystallographic two-fold axis running through the Gd · · · Cu(3) vector, which leads to two distinct copper environments. Atom Cu(3) is bound to two N- and two O-donors from chp ligands, with the two O atoms shared with the Gd atom. The geometry is therefore *cis*, however there is a considerable distortion from a square geometry at Cu(3), with a dihedral angle of 26° between the O–Cu–O and N–Cu–N planes. The remaining two copper sites [Cu(1) and Cu(2)] both have an N_3O donor set and co-ordination geometries much closer to square planar. The Cu–O and Cu–N bond lengths are unexceptional.

The Gd atom is eight-co-ordinate, bound to six chp O atoms, two of which [O(3r) and O(6r)] are shared with Cu(3), and two O-donors from a nitrate group. The Gd-O distances to the nitrate oxygens and the two μ-O-atoms are longer (2.475–2.513 Å) than those to the remaining chp oxygens (2.266–2.283 Å). The chp ligands in **6** adopt two distinct co-ordination modes, bi- and tri-nucleating, with the N-donors bound exclusively to copper centres.

Table 5 Selected bond lengths (Å) and angles (°) in compounds **6** and **11**

	6 Ln = Gd	**11** Yb		**6** Gb	**11** Yb
Ln-O(1r)	2.266(8)	2.192(6)	Ln-O(6r)	2.459(8)	2.408(6)
Ln-O(2r)	2.269(9)	2.176(6)	Ln-O(3r)	2.475(9)	2.372(6)
Ln-O(7r)	2.280(8)	2.200(6)	Ln-O(12n)	2.487(9)	2.440(6)
Ln-O(8r)	2.283(9)	2.223(7)	Ln-O(11n)	2.513(9)	2.504(7)
Cu(1)–O(5r)	1.983(8)	1.933(6)	Cu(2)–N(3r)	1.995(10)	2.018(7)
Cu(1)–N(6r)	2.002(10)	2.028(7)	Cu(2)–N(1r)	2.042(10)	2.044(7)
Cu(1)–N(7r)	2.009(10)	1.996(7)	Cu(3)–O(6r)	1.953(8)	1.963(6)
Cu(1)–N(8r)	2.027(10)	—	Cu(3)–O(3r)	1.961(8)	1.959(6)
Cu(1)–O(21n)	—	1.987(7)	Cu(3)–N(4r)	1.973(11)	1.983(7)
Cu(2)–O(4r)	1.974(9)	1.960(6)	Cu(3)–N(5r)	1.983(10)	1.997(7)
Cu(2)–N(2r)	1.985(10)	1.995(7)			
O(5r)–Cu(1)–N(6r)	88.8(4)	91.2(3)	N(2r)–Cu(2)–N(3r)	171.9(4)	172.1(3)
O(5r)–Cu(1)–N(7r)	83.2(4)	90.3(3)	O(4r)–Cu(2)–N(1r)	178.4(4)	178.8(3)
N(6r)–Cu(1)–N(7r)	169.6(4)	161.4(3)	N(2r)–Cu(2)–N(1r)	95.4(4)	96.6(3)
O(5r)–Cu(1)–N(8r)	179.0(3)	—	N(3r)–Cu(2)–N(1r)	90.8(4)	88.9(3)
N(6r)–Cu(1)–N(8r)	91.7(4)	—	O(6r)–Cu(3)–O(3r)	81.1(4)	79.5(2)
N(7r)–Cu(1)–N(8r)	96.4(4)	—	O(6r)–Cu(3)–N(4r)	160.7(4)	94.5(3)
O(5r)–Cu(1)–O(21n)	—	170.8(3)	O(3r)–Cu(3)–N(4r)	92.9(4)	94.5(3)
N(6r)–Cu(1)–O(21n)	—	89.3(3)	O(6r)–Cu(3)–N(5r)	92.4(4)	96.8(3)
N(7r)–Cu(1)–O(21n)	—	92.1(3)	O(3r)–Cu(3)–N(5r)	158.5(4)	161.0(3)
O(4r)–Cu(2)–N(2r)	86.2(4)	84.5(3)	N(4r)–Cu(3)–N(5r)	99.4(4)	95.1(3)
O(4r)–Cu(2)–N(3r)	87.6(4)	89.9(3)			

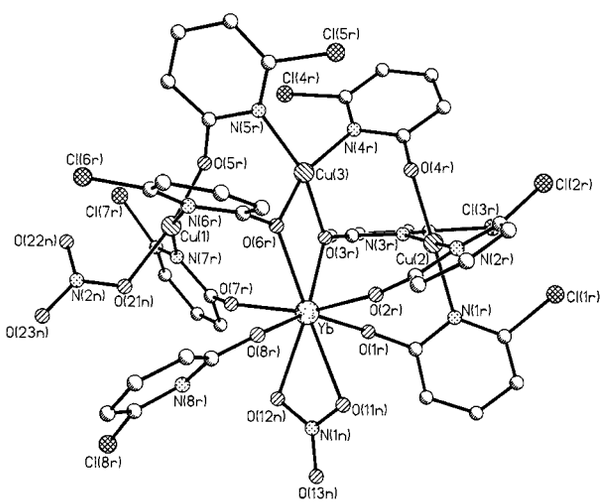

Fig. 4 Structure of complex **11** in the crystal, with the numbering scheme adopted

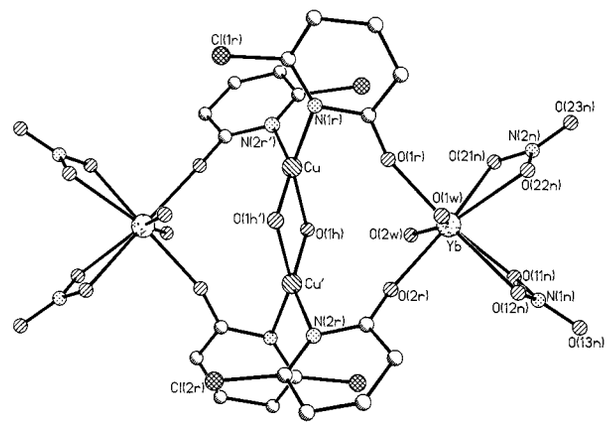

Fig. 5 Structure of complex **13** in the crystal, with the numbering scheme adopted

The structure of $[Cu_3Yb(chp)_7(Hchp)(NO_3)_2]$ **11** is closely related to that of **6**, differing in that three distinct copper sites are found (Fig. 4). Atom Cu(3), which again shares two O atoms with the Yb, and Cu(2) have very similar co-ordination environments to their counterparts in **6**. The major change is at Cu(1), where the N-donor of one of the formerly binucleating chp groups has been replaced by a monodentate nitrate group, leading to a *trans* N_2O_2 donor set. The geometry at Cu(1) is markedly distorted from square planar, with a dihedral angle of 20° between any pair of N–Cu–O planes. The ytterbium site is eight-co-ordinate, with one of the eight O-donors derived from the terminal Hchp ligand. The Yb–O bond lengths are shorter than the equivalent Gd–O bond lengths in **6** (Table 5), with the bonds to mono- and bi-nucleating chp ligand shorter (2.18–2.22 Å) than those to two O atoms of trinucleating chp groups (2.37 and 2.41 Å) while the bonds to the nitrate oxygens are still longer (2.44 and 2.50 Å). There is some disorder in the terminal Hchp group, and no evidence of significant hydrogen bonding involving the H atom attached to the ring nitrogen.

These structures strongly resemble the complexes isolated from CH_2Cl_2–MeOH when **2** is treated with $Ln(NO_3)_3{\cdot}xH_2O$ (Ln = Gd, Dy or Er).[11] However when **2** is treated with hydrated ytterbium nitrate in thf crystals are found which contain a Type I complex, $[\{CuYb(\mu\text{-}OH)(chp)_2(NO_3)_2(H_2O)_2\}_2]$ **13** (Fig. 5) which crystallises as a thf solvate. The centrosymmetric structure contains a central Cu_2O_2 ring with the O atoms derived from hydroxide groups. There are two possible sources of hydroxide, either the waters of crystallisation of the lanthanoid starting material or the solvent. The two copper sites are four-co-ordinate, with the remaining sites on each Cu occupied by N-donors from chp groups. This leads to an N_2O_2 donor set, which has a *cis* geometry, but the dihedral angle of 39° between the N–Cu–N and O–Cu–O planes is almost midway between that required for a regular square-planar or tetrahedral environment.

The chp ligands attach two eight-co-ordinate Yb atoms to this dinuclear copper core. The eight donor atoms are derived from two chp ligands, four O atoms from two bidentate nitrates and two water molecules, presumably retained from the starting salt. As found for complexes **6** and **11**, the bonds to chp oxygen donors are the shortest with those to nitrate oxygens the longest (Table 6). The water molecules attached to Yb are involved in hydrogen bonding to thf solvate molecules [O(2w) · · · O(11) 2.70(3), O(1w) · · · O(21) 2.85(3) Å], to the μ-hydroxides attached to Cu [O(2w) · · · O(1h) 2.70(3) Å] and to nitrate anions in neighbouring molecules [O(1w) · · · O(12n′) 2.85(3) Å].

When complex **2** is treated with hydrated ytterbium nitrate in

Table 6 Selected bond lengths (Å) and angles (°) in compounds **13** and **18**

	13 Ln = Yb	**18** Er		**13** Yb	**18** Er
Ln–O(1r)	2.18(2)	2.217(12)	Ln–O(12n)	2.490(14)	2.450(12)
Ln–O(2r)	2.15(2)	2.245(12)	Ln–O(21n)	2.41(2)	2.426(13)
Ln–O(11n)	2.40(2)	2.426(13)	Ln–O(22n)	2.36(2)	2.453(12)
Ln–O(1w)	2.30(2)	—	Ln–O(2w)	2.288(14)	—
Ln–O(3r)	—	2.275(13)	Ln–(4r)	—	2.255(12)
Cu–O(1h)	1.964(13)	1.953(12)	Cu–N(1r)	1.97(2)	2.02(2)
Cu–O(1h′)	1.958(13)	1.964(11)	Cu–N(2r′)	2.00(2)	1.999(13)
Cu · · · Cu(a)	2.927(6)	2.929(6)			
O(1h)–Cu–O(1h′)	83.5(6)		O(1h′)–Cu–N(1r)	97.7(6)	
O(1h)–Cu–N(1r)	151.5(6)		O(1h′)–Cu–N(2r′)	152.0(6)	
O(1h)–Cu–N(2r′)	95.2(6)		N(1r)–Cu–N(2r′)	96.5(7)	

Table 7 Selected bond lengths (Å) and angles (°) in compounds **15**, **19**, **21** and **22**

	15 Ln = Yb		**19** Pr	**21** Gd	**22** Er	
	Molecule 1	Molecule 2			Molecule 1	Molecule 2
Ln–O(1r)	2.179(7)	2.189(7)	2.367(6)	2.254(6)	2.193(12)	2.218(11)
Ln–O(2r)	2.192(7)	2.183(7)	2.341(5)	2.235(5)	2.179(11)	2.202(11)
Ln–O(2m)	2.322(8)	2.309(7)	2.524(7)	2.443(6)	2.357(12)	2.360(12)
Ln–O(3m)	2.291(7)	2.297(8)	2.494(5)	2.358(6)	2.313(11)	2.327(12)
Ln–O(4m)	—	—	2.447(5)	—	—	—
Ln–O(11n)	2.420(8)	2.364(8)	2.668(6)	2.491(6)	2.442(12)	2.450(12)
Ln–O(12n)	2.379(8)	2.378(8)	2.535(9), 2.648(9)	2.442(6)	2.374(13)	2.382(12)
Ln–O(21n)	2.388(8)	2.434(9)	2.559(5)	2.456(6)	2.400(12)	2.410(12)
Ln–O(22n)	2.380(7)	2.366(9)	2.433(9), 2.829(9)	2.472(6)	2.404(12)	2.429(13)
Cu–O(1m)	1.943(6)	1.947(7)	1.950(4)	1.958(6)	1.942(11)	1.928(11)
Cu–O(1m′)	1.959(6)	1.953(7)	1.952(4)	1.963(5)	1.951(11)	1.964(11)
Cu–N(1r)	1.965(8)	1.983(8)	1.999(5)	2.000(7)	1.980(14)	1.980(14)
Cu–N(2r′)	1.991(8)	1.965(9)	2.009(5)	1.992(7)	1.976(13)	1.972(12)
Cu · · · Cu′	2.944(2)	2.935(2)	2.959(2)	2.944(2)	2.945(8)	2.947(7)
O(1m)–Cu–O(1m′)	82.1(3)	82.4(3)	81.4(2)	82.7(3)	81.7(5)	81.6(5)
O(1m)–Cu–N(1r)	96.9(3)	97.8(3)	149.4(2)	152.8(3)	150.6(5)	151.8(5)
O(1m)–Cu–N(2r′)	151.5(3)	150.4(3)	98.6(2)	96.8(3)	98.6(5)	98.0(5)
O(1m′)–Cu–N(1r)	150.4(3)	149.4(3)	98.1(2)	96.9(3)	96.7(5)	95.9(5)
O(1m′)–Cu–N(2r′)	96.9(3)	95.6(3)	148.1(2)	149.2(3)	150.3(5)	149.5(5)
N(1r)–Cu–N(2r′)	97.5(3)	98.5(4)	97.4(2)	97.0(3)	96.9(6)	98.0(5)
Angle between N–Cu–N and O–Cu–O planes			43.6(3)	40.4(3)	41.2(6)	40.5(2)

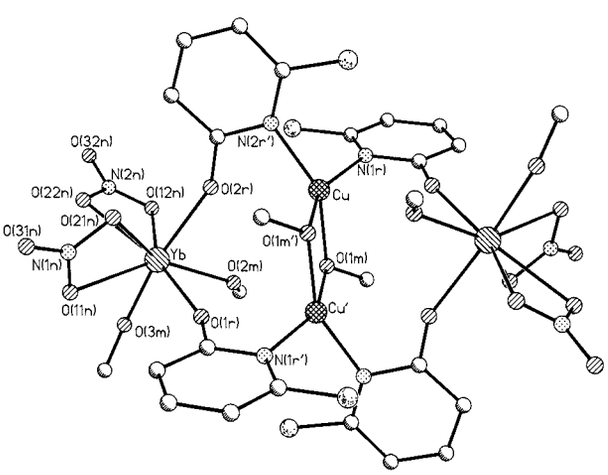

Fig. 6 Structure of complex **15** in the crystal, with the numbering scheme adopted. Complexes **21** and **22** are isostructural, differing only in the pyridonate derivative and the same numbering scheme applies to them

CH_2Cl_2–MeOH green crystals are formed which contain a further Type I complex $[\{CuYb(\mu\text{-}OMe)(chp)_2(NO_3)_2(MeOH)_2\}_2]$ **15** (Fig. 6). The structure contains two nearly identical molecules in the asymmetric unit. At the centre of each molecule is a Cu_2O_2 molecule, with the oxygen atoms now derived from deprotonated MeOH. Each copper co-ordination sphere is completed by two N-donors from chp groups, leading to a *cis* N_2O_2 donor set, although again there is a considerable dihedral angle between the N–Cu–N and O–Cu–O planes (*ca*. 40°). The chp groups bridge on to the Yb atoms which are found at the periphery of the molecule. Each ytterbium site is eight-co-ordinate, bound to two O atoms from the linking chp units, four O atoms from two bidentate nitrate and two MeOH molecules. Again a range of Yb–O bond lengths is found, dependent on the source of the O-donor; the Yb–O (chp) bonds are markedly shorter than those from other ligands (Table 7).

These results, combined with those reported in ref. 11 suggested that while Type I complexes are found with chp ligands when the rare earth is ytterbium, Type II complexes are more common, certainly for lighter lanthanoids. For the mhp ligand only Type I complexes have been found.[10] It is conceivable that

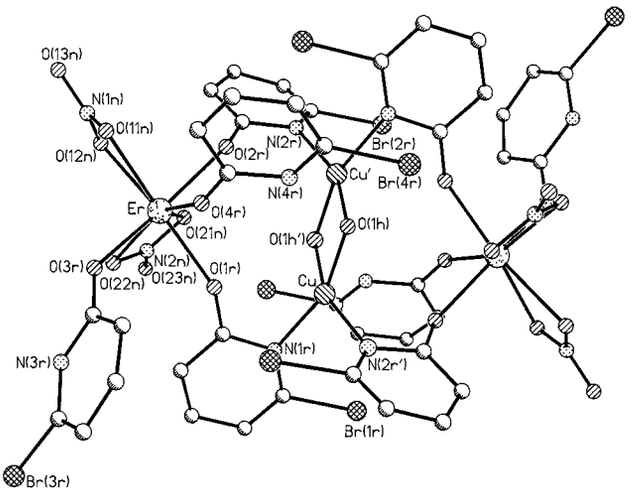

Fig. 7 Structure of complex **18** in the crystal, with the numbering scheme adopted

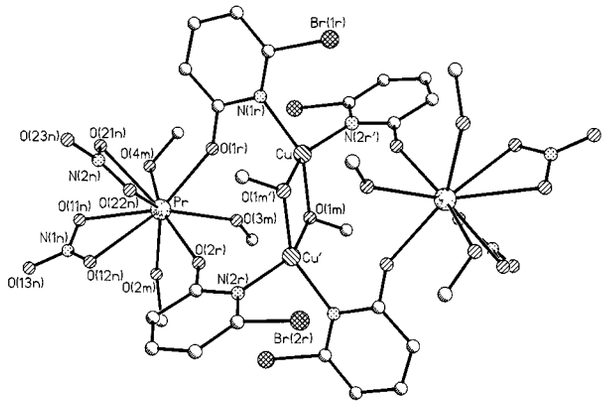

Fig. 8 Structure of complex **19** in the crystal, with the numbering scheme adopted

this difference is related to the electronegativity of the 6-substituent of the pyridonate ligand, which is known to modify the basicity of the ring nitrogen. We therefore examined reactions of the 6-bromo-2-pyridone ligand (Hbhp), which should have properties intermediate between those of Hchp and Hmhp.

Reactions of complex 3 with lanthanoid nitrates

Reaction of $[Cu_2(bhp)_4]$ **3** with lanthanoid nitrates in CH_2Cl_2 leads to both Type I and II complexes, depending on the lanthanoid used. For early 4f elements, *e.g.* samarium **16** and gadolinium **17**, Type II complexes are found. Unfortunately single crystals of **16** and **17** could not be obtained, however elemental analysis and FAB mass spectral results provide sufficient evidence to allow the formulae to be assumed.

For heavier lanthanoids, crystals of Type I complexes could be obtained. For example, $[\{CuEr(\mu\text{-}OH)(bhp)_2(NO_3)_2(Hbhp)_2\}_2]$ **18** is obtained if erbium nitrate is used (Fig. 7). In many ways this resembles the structure of **13** in that a central Cu_2O_2 ring, containing μ-hydroxides, is bridged to two peripheral eight-co-ordinate erbium atoms by pyridonate ligands, in this case bhp. There is a minor difference in the dinuclear copper core in that the dihedral angle between the N–Cu–N and O–Cu–O planes at each copper is only 29.4°, smaller than in **13**. The main difference is in the co-ordination sphere of the rare-earth atom. In **18** the eight O-donors are derived from two bridging bhp ligands, four from two bidentate nitrates and the final two from terminal Hbhp ligands. The Er–O (bhp) bonds are shorter than Er–O (NO_3) bonds (Table 6). The terminal Hbhp ligands are both involved in hydrogen bonds, as were the water molecules attached to Yb in **13**. One Hbhp has an intramolecular contact to a μ-hydroxide [N(4r)···O(1h) 2.664(13) Å] while the second has an intermolecular contact to a nitrate group in a neighbouring molecule [N(3r)···O(12n′) 2.89(2) Å].

If the reactions of complex **3** are carried out in CH_2Cl_2–MeOH the crystalline products obtained are Type I for all rare earths investigated. Complexes of stoichiometry $[\{CuLn(\mu\text{-}OMe)(bhp)_2(NO_3)_2(MeOH)_3\}_2]$ (Ln = Pr **19** or Nd **20**) or $[\{CuLn(\mu\text{-}OMe)(bhp)_2(NO_3)_2(MeOH)_2\}_2]$ (Ln = Gd **21** or Er **22**) could be crystallised, differing only in the co-ordination number of the peripheral Ln atom. The lighter lanthanoids are nine-co-ordinate (Fig. 8), while the heavier are eight-co-ordinate, giving rise to structures identical to those of **15** differing only in the pyridonate derivative used (Fig. 6). The additional ligand attached to the lanthanoid centre in **19** and **20** is a terminal MeOH. Bond lengths and angles for these complexes are given in Table 7. The reactivity of **3** is therefore more akin to that of **1** than that of **2**, in that Type I complexes are much more common than Type II. The only Type II complexes found are for early lanthanoids in the absence of MeOH; for later lanthanoids Type I complexes are found containing either hydroxide or methoxide bridges within the central Cu_2O_2 ring. Combined with the observation that for the chp ligand Type I complexes are only found for ytterbium this suggests that the heavier rare earths favour the Cu_2Ln_2 stoichiometry.

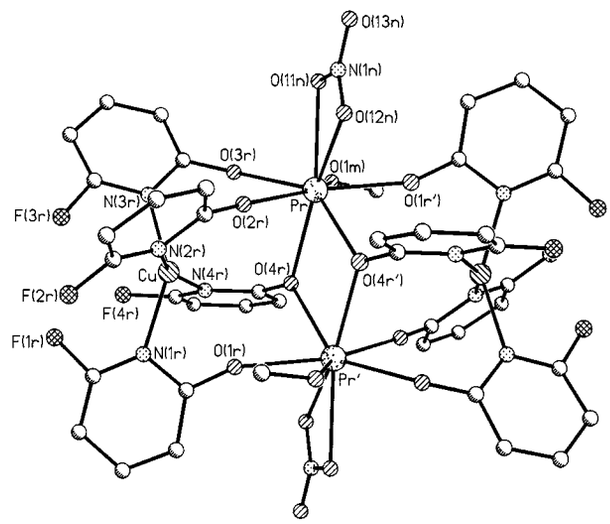

Fig. 9 Structure of complex **23** in the crystal, with the numbering scheme adopted. The numbering scheme also applies to complex **25** which is isostructural

Reactions of complex 4 with lanthanoid nitrates

The 6-fluoro-2-pyridonate ligand has been found to have different chemistry to the 6-chloro- and 6-bromo-derivatives. For example complex **4** crystallises as a tetranuclear 'dimer of dimers' compared with the simpler dinuclear structures of **2** and **3**.[14] The reactivity of **4** is also different to that of **2** and **3**, leading to a new structural type.

Using CH_2Cl_2–MeOH as the solvent system gives green crystals of stoichiometry $[\{CuLn(fhp)_4(NO_3)(MeOH\}_2]$ (Ln = Pr **23**, Gd **24** or Yb **25**). The structure is centrosymmetric containing a central Ln_2O_2 ring, with these μ-O atoms derived from fhp ligands (Fig. 9). These fhp ligands bridge on to the Cu atoms of the structure through the ring N-donors, thus these units are trinucleating. The Ln···Cu vectors are further bridged by binucleating fhp ligands, with these pyridonates binding to the lanthanoid site through the O atom and to Cu through the nitrogen. The Ln···Cu vector is bridged by two such ligands, the Ln···Cu(a) contact by one such binucleating unit.

The copper site in these structures is four-co-ordinate, bound

Table 8 Selected bond lengths (Å) and angles (°) in compounds **23** and **25**

	23 Ln = Pr	**25** Yb		**23** Pr	**25** Yb
Ln–O(1ra)	2.326(4)	2.16(2)	Ln–O(4ra)	2.511(4)	2.39(2)
Ln–O(2r)	2.341(4)	2.20(2)	Ln–O(1m)	2.520(5)	2.42(3)
Ln–O(3r)	2.386(4)	2.23(2)	Ln–O(11n)	2.582(5)	2.43(2)
Ln–O(4r)	2.428(4)	2.27(2)	Ln–O(12n)	2.600(5)	2.47(2)
Cu–N(1r)	2.025(5)	2.01(3)	Cu–N(3r)	2.028(5)	1.99(2)
Cu–N(2r)	1.987(5)	1.99(2)	Cu–N(4r)	2.008(5)	2.01(3)
N(1r)–Cu–N(2r)	96.3(2)	96.3(10)	N(2r)–Cu–N(3r)	90.9(2)	92.6(9)
N(1r)–Cu–N(3r)	146.1(2)	150.9(10)	N(2r)–Cu–N(4r)	160.1(2)	160.6(9)
N(1r)–Cu–N(4r)	90.6(2)	89.8(10)	N(3r)–Cu–N(4r)	92.1(2)	92.6(9)

Table 9 Angles (°) within co-ordination polyhedra for lanthanoid complexes with dodecahedral geometries

	Compound								
	6 Ln = Gd	**11** Yb	**13** Yb	**15** Yb	**18** Er	**21** Gd	**22** Er	**23** Pr	**25** Yb
Angles within intersecting trapezia	106.7	106.8	102.0	104.0	103.1	100.2	102.9	102.0	104.3
	107.1	108.1	104.3	111.3	111.9	101.8	110.3	102.8	105.5
	111.6	109.6	111.9	111.9	111.9	102.3	108.2	108.2	110.3
	114.1	114.9	112.3	112.7	114.3	112.9	116.0	110.9	111.7
Mean deviation of atoms from trapezia mean plane/ Å	0.195	0.162	0.042	0.029	0.137	0.096	0.082	0.174	0.070
Maximum deviation of atoms from trapezia mean plane/ Å	0.350	0.200	0.063	0.064	0.213	0.254	0.171	0.243	0.102
Angle between mean planes of trapezia	93.2	88.3	93.3	89.8	86.4	87.9	89.4	94.1	92.1

exclusively to N-donors from fhp. The geometry shows a distortion from square planar, again through a large dihedral angle between any two N–Cu–N planes (*ca.* 38°) (Table 8).The lanthanoid site is eight-co-ordinate, with the O-donors derived from two trinucleating fhp, three binucleating fhp, one bidentate nitrate and one MeOH ligand. As in all previous structures the bonds to binucleating fhp ligands are the shortest in the lanthanoid co-ordination sphere, with bonds to the bidentate nitrate group the longest. As expected, based on the lanthanoid contraction, the Ln · · · O bond lengths are shorter for Ln = Yb than for Pr.

The structures of complexes **23**–**25** resemble that of $[\{CuLa(chp)_4(Hchp)(NO_3)\}_2]$ **26**, formed from the reaction of **2** with hydrated lanthanum nitrate.[9] This complex was formed in very low yield, and crystallised over a period of 13 months. Here the yields are much higher and the complex can be isolated in days. There are two main differences between **23**–**25** and **26**. First, the MeOH solvate attached to Ln in **23**–**25** is replaced in **26** by a molecule of Hchp. Secondly, one of the bridging chp groups in **26** binds to La through the ring N atom in addition to the exocyclic oxygen. This was unexpected, and the reason for the adoption of this bonding mode in **26** remains unclear, especially as we have now crystallised closely related species where more normal bonding by the pyridonate ligand is observed.

FAB mass spectroscopic studies

Crystallographic characterisation remains the only unambiguous tool in assigning structure to such complicated molecules. However, we have found a trend in the mass spectroscopic properties which, when taken in conjunction with elemental analysis results, allows us to assign structure in these molecules.

Type I complexes, which contain Cu_2Ln_2 cores, do not give any significant peaks in the FAB mass spectrum under standard conditions. Conversely Type II complexes almost invariably give interpretable fragmentation patterns, although rarely is the molecular ion observed. In particular the peak for $[Cu_3Ln(xhp)_5]^+$ is always intense and its presence is diagnostic that a Type II structure is present. It is unclear why Type II complexes should give much better mass spectra than other structural types. It is possible that the presence of many more bridging xhp ligands in Type II than in Type I complexes (seven or eight rather than four xhp ligands respectively) is imparting greater stability.

Discussion

Lanthanoid co-ordination geometries

In all except two of the structurally characterised complexes reported here the lanthanoid site is eight-co-ordinate. The exceptions are compounds **5** and **19**. The geometry about this metal site is irregular, but approximates most closely to dodecahedral (Fig. 10). Such a geometry can be described in terms of two mutually perpendicular trapezia, and parameters consistent with such a description are given in Table 9.

The dodecahedron is the closest-packed eight-vertex polyhedron, and we were curious whether the geometry showed any distortion dependent on the lanthanoid centre present. As is well known the radii of 4f elements decrease as the series is traversed, and therefore the geometry might be comparatively regular for metal centres of a specific radius, and more distorted for either larger or smaller lanthanoid atoms. Given the structural complexity of these co-ordination sites, which each involves a mixture of chelating, bridging and terminal ligands, and with ligands of different size, any conclusion is likely to be slightly ambiguous.

Of the structural parameters in Table 9 the mean and maximum deviations of O atoms from the mean planes of the trapezia containing them show the most interesting trends. Two factors are apparent. First the lanthanoid sites in the Type II complexes (**6** and **11**) are considerably more distorted, for a given Ln, from dodecahedral than the equivalent sites in Type I complexes (*cf.* **6** with **21**, or **11** with **13** or **15**). The Type II lanthanoid sites feature two O atoms from a bidentate ligand, with six O-donors from bridging chp ligands in **6** and five O-donors from bridges plus one oxygen from a terminal chp in **11**. By comparison Type I structures have two bidentate ligands, two O-donors from bridges and two terminal O atoms. The implication, which is perhaps unexpected, is that bridging lig-

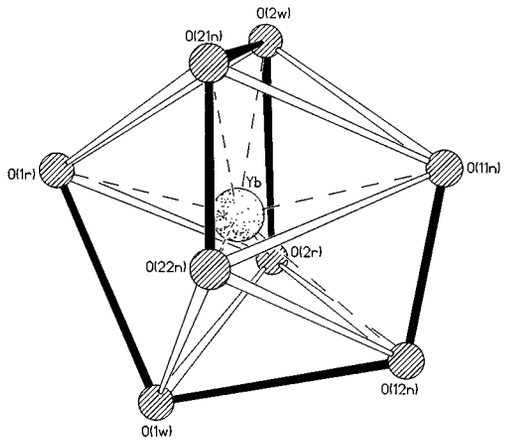

Fig. 10 The co-ordination polyhedra about Yb in complex **13**, illustrating the dodecahedral geometry. The two mutually perpendicular trapezia are shown in full lines, the other O···O contacts within the dodecahedron with open lines

ands impose more distortion than chelating nitrate groups with these metal atoms with high co-ordination numbers. The complexes of stoichiometry $[\{CuLn(fhp)_4(NO_3)(MeOH)\}_2]$ **23** and **25** appear to be intermediate.

The second observation is more clear-cut. Where similar structures are found the co-ordination site containing the smaller lanthanoid is the less distorted from dodecahedral (*cf.* **6** with **11**, or **21** with **22**, or **23** with **25**). This is further amplified by complex **19**, which contains a nine-co-ordinate praseodymium site but which is otherwise equivalent to **21** and **22**. Here there is a change from a tricapped trigonal-prismatic geometry (as found for Pr in **19**) to distorted dodecahedral (for Gd in **21**) to a less distorted dodecahedral geometry for heavier rare earths (*e.g.* Er in **22**). In related studies of $[\{CuLn(\mu\text{-}OMe)(mhp)_2(NO_3)_2(Hmhp)(MeOH)_x\}_2]$ complexes[10] we found a similar change in co-ordination number at samarium.

Trends in structural type

Although the smaller polynuclear complexes reported here belong to three distinct structural classes there is a clear relationship between the Type II complexes and the structures (**23** and **25**) formed with the fhp ligand. In each case four metal centres are held together by xhp ligands with the co-ordination spheres of the lanthanoid centres completed by terminal solvates and bidentate nitrates. Type I complexes are quite distinct in that deprotonated solvent or hydroxides play an important structural role in bridging the central Cu···Cu vector.

The trends in overall structure are worth considering. Where the pyridonate ligand has a highly electronegative substituent in the 6 position structures are found (either Type II or **23** and **25**) where the Cu–Ln cage is held together through the ligand only, with little interference from solvent molecules. This is true for all three lanthanoid centres studied with the fhp ligand (complexes **23**–**25**), however with the chp ligand once Yb is reached the presence of MeOH leads to a Type I complex. With the mhp ligand, where there is no electronegative substituent, Type I complexes are formed in the presence of MeOH for all lanthanoid centres investigated,[10] while for the intermediate bhp ligand the change from Type II to I occurs between Gd and Er. {Although no structure determination for $[Cu_3Gd(bhp)_8(NO_3)]$ **17** was performed, elemental analysis and FAB mass spectral results allow us to be confident in assigning structure.} The tendency for later lanthanoids to favour Type I complexes may be related to co-ordination geometry; it appears (see above) that Type I complexes allow more regular dodecahedral lanthanoid co-ordination sites, which are also more favourable for the heavier metals.

It is therefore possible to suggest that the structure found is controlled by two competing trends. Highly electron-withdrawing groups in the 6 position of the pyridonate appear to favour complexes where the tetranuclear heterometallic array is bridged exclusively by xhp ligands, while small, late rare-earth centres prefer Type I structures. For the chp and bhp ligands these interactions are sufficiently closely balanced for a change in overall structure to occur as the 4f series is traversed. For the mhp and fhp ligands the balance lies to one side or the other, and the structure is largely maintained throughout the rare earths.

Acknowledgements

We thank the EPSRC (SERC) for studentships (to C. M. G. and P. E. Y. M.) and a post-doctoral fellowship (for S. P.) and for funding for a diffractometer. We are also grateful to Professor J. A. K. Howard and Dr. R. Copley at the University of Durham for access to the CCD diffractometer and X-ray data collection for complex **23**.

References

1 (*a*) A. Bencini, C. Benelli, A. Caneschi, R. L. Carlin, A. Dei and D. Gatteschi, *J. Am. Chem. Soc.*, 1985, **107**, 8128; (*b*) C. Benelli, A. Caneschi, D. Gatteschi, O. Guillou and L. Pardi, *Inorg. Chem.*, 1990, **29**, 1751 and refs. therein.
2 N. Matsumato, M. Sakamoto, H. Tamaki, H. Okawa and S. Kida, *Chem. Lett.*, 1989, 853.
3 D. M. L. Goodgame, D. J. Williams and R. E. P. Winpenny, *Polyhedron*, 1989, **8**, 1531.
4 M. Andruh, I. Ramade, E. Codjovi, O. Guillou, O. Kahn and J. C. Trombe, *J. Am. Chem. Soc.*, 1993, **115**, 1822 and refs. therein.
5 S. Wang, S. J. Trepanier and M. J. Wagner, *Inorg. Chem.*, 1993, **32**, 833.
6 A. J. Blake, P. E. Y. Milne, P. Thornton and R. E. P. Winpenny, *Angew. Chem., Int. Ed. Engl.*, 1991, **30**, 1139.
7 A. J. Blake, R. O. Gould, P. E. Y. Milne and R. E. P. Winpenny, *J. Chem. Soc., Chem. Commun.*, 1991, 1453.
8 A. J. Blake, R. O. Gould, P. E. Y. Milne and R. E. P. Winpenny, *J. Chem. Soc., Chem. Commun.*, 1992, 522.
9 A. J. Blake, P. E. Y. Milne and R. E. P. Winpenny, *J. Chem. Soc., Dalton Trans.*, 1993, 3727.
10 A. J. Blake, V. A. Cherepanov, A. A. Dunlop, C. M. Grant, P. E. Y. Milne, J. M. Rawson and R. E. P. Winpenny, *J. Chem. Soc., Dalton Trans.*, 1994, 2927.
11 C. Benelli, A. J. Blake, P. E. Y. Milne, J. M. Rawson and R. E. P. Winpenny, *Chem. Eur. J.*, 1995, **1**, 614.
12 J.-P. Costes, F. Dahan, A. Dupuis and J.-P. Laurent, *Inorg. Chem.*, 1996, **35**, 2400.
13 X.-M. Chen, Y.-L. Wu, U.-X. Tong and X.-Y. Huang, *J. Chem. Soc., Dalton Trans.*, 1996, 2443.
14 A. J. Blake, C. M. Grant, F. E. Mabbs, E. J. L. McInnes, P. E. Y. Milne, S. Parsons, J. M. Rawson and R. E. P. Winpenny, *J. Chem. Soc., Dalton Trans.*, 1996, 4077.
15 G. M. Sheldrick, SHELX 76, University of Cambridge, 1976.
16 G. M. Sheldrick, SHELXL 93, University of Göttingen, 1993.
17 J. Cosier and A. M. Glazer, *J. Appl. Crystallogr.*, 1986, **19**, 105.
18 W. Clegg, *Acta Crystallogr., Sect. A*, 1981, **37**, 22.
19 N. Walker and D. Stuart, DIFABS, program for applying empirical absorption corrections, *Acta Crystallogr., Sect. A*, 1983, **39**, 158.
20 G. M. Sheldrick, SHELXS 86, program for crystal structure solution, *Acta Crystallogr., Sect. A*, 1990, **46**, 467.

Received 5*th September* 1996; *Paper* 6/06126F